Phys Chem Minerals (2003) 30: 293 – 304
DOI 10.1007/s00269-003-0305-7

ORIGINAL PAPER

E. J. Palin · M. T. Dove · S. A. T. Redfern
C. I. Sainz-Díaz · W. T. Lee

Computational study of tetrahedral Al–Si and octahedral Al–Mg ordering in phengite

Received: 8 August 2002 / Accepted: 14 February 2003

Abstract As part of a wider study of the nature and origins of cation order–disorder in micas, a variety of computational techniques have been used to investigate the nature of tetrahedral and octahedral ordering in phengite, $K_2^{[6]}(Al_3Mg)^{[4]}(Si_7Al)O_{20}(OH)_4$. Values of the atomic exchange interaction parameters J_n used to model the energies of order–disorder were calculated. Both tetrahedral Al–Si and octahedral Al–Mg ordering were studied and hence three types of interaction parameter were necessary: for T–T, O–O and T–O interactions (where T denotes tetrahedral sites and O denotes octahedral sites). Values for the T–T and O–O interactions were taken from results on other systems, whilst we calculated new values for the T–O interactions. We have demonstrated that modelling the octahedral and tetrahedral sheets alone and independently produces different results from modelling a whole T–O–T layer, hence justifying the inclusion of the T–O interactions. Simulations of a whole T–O–T layer of phengite indicated the presence of short-range order, but no long-range order was observed.

Keywords Phengite · Cation ordering · Layer silicates · Phase transitions · Monte Carlo simulations

E. J. Palin · M. T. Dove (✉) · S. A. T. Redfern · W. T. Lee
Department of Earth Sciences,
University of Cambridge, Downing Street,
Cambridge CB2 3EQ, UK
e-mail: martin@esc.cam.ac.uk

C. I. Sainz-Díaz
Departamento de Ciencias de la Tierra y Química Ambiental,
Estación Experimental del Zaidín (CSIC),
C/ Profesor Albareda, 1, 18008-Granada, Spain

W. T. Lee
Mineralogisch-Petrographisches Institut,
Universität Hamburg, Grindelallee 48,
20146 Hamburg, Germany

Introduction

The mica group of minerals has a wide range of chemical stabilities, due to the ability of the structure to accommodate a wide range of cationic substitutions in the sites within the octahedral (O) and tetrahedral (T) sheets, as well as in the interlayer region. Aside from variations in the cation site occupancies of six- and fourfold sites of the structure, different stacking sequences and rotations of the T–O–T layers lead to polytypic variations.

Interest in order–disorder in phengites has arisen from attempts to rationalize the thermobaric controls on the formation of specific polytypes, the stability of which may also be related to cation ordering in both the T and O layers. In both the 3T and $2M_1$ polytypes there are two symmetrically distinct tetrahedral sites, T1 and T2, whereas the octahedral sites split into three distinct sites (designated M1, M2 and M3) in the 3T phengite structure, and only one in $2M_1$ phengite (M2 and M3 become equivalent by symmetry, and M1 is empty).

Order–disorder on the tetrahedral and octahedral sites of phengite 3T has been studied as a function of temperature using neutron diffraction by Pavese et al. (1997), who suggested the occurrence of order in both the tetrahedral and octahedral sites, independent of temperature, as had been suggested previously from petrological observations of the relative stability of polytypes (Sassi et al. 1994 had suggested that the 3T phengite was more ordered as a result of its high-pressure environment of formation). Pavese et al. (1999) then studied the tetrahedral order–disorder in a natural phengite $2M_1$, measuring disorder at ambient conditions, followed by a small degree of ordering upon heating. Pavese et al. (2000) reconsidered the cation partitioning in phengite 3T on the basis of data collected from a different neutron instrument. Their revised results were in full agreement with their earlier measurement of octahedral order, but suggested that the degree of tetrahedral order was lower than they had previously thought. Ivaldi et al. (2001) studied a sample

of coexisting phengite $2M_1$ and 3T using EMPA and single-crystal X-ray diffraction, and concluded from bond-length measurements that tetrahedral order was absent in both polytypes, but that in the phengite 3T there was partial octahedral order. Mookherjee et al. (2001) studied a phengite $2M_1$ at high temperature by neutron diffraction, but found no evidence for any cation readjustment upon heating.

The experimental measurements of phengites by neutron diffraction push against the limits of the technique for resolving small changes in occupancies across the cation sites within these low-symmetry large unit-cell structures, and show that the controls on cation ordering still remain to be resolved. Here, we address this question using the computational methods adopted earlier for muscovite (Palin et al. 2001), and explore the relationship between the ordering in both the T and the O layers of phengite. In doing so, we attempt to determine the strength of coupling within layers, and to identify the important interactions that control the ordering patterns.

In a previous paper (Palin et al. 2001) we discussed cation ordering in muscovite, $K_2{}^{[6]}Al_4{}^{[4]}(Si_6Al_2)O_{20}(OH)_4$. We showed that computational techniques could be used successfully to model muscovite, which was a step forward in the field owing to the hydrous nature of muscovite and its dilute Al:Si ratio. Here, we extend our work to phengite, $K_2{}^{[6]}(Al_3Mg)^{[4]}(Si_7Al)\ O_{20}(OH)_4$, which is closely related to muscovite (via the substitution $^{[4]}Si^{[6]}Mg^{[6]}Al_{-1}{}^{[4]}Al_{-1}$), but which has three ordering cation species and hence is more complicated to model. The structure of the mineral is shown in Fig. 1; it consists of sheets of AlO_6 and MgO_6 octahedra (with some O being replaced by OH), sandwiched between two sheets of SiO_4 and AlO_4 tetrahedra. Such structural units are referred to as layers, and adjacent layers are separated by a sheet of K cations. We consider in this work the ordering of Al and Si across tetrahedral sites, and the ordering of Al and Mg across octahedral sites.

In muscovite, we simulated both a single tetrahedral sheet and a series of T–O–T layers, with the latter simulations including interactions between tetrahedral sheets in adjacent layers and adjacent tetrahedral sheets in the same layer. However, we discovered that in a multilayer simulation starting from a completely random initial configuration, the order produced was two-dimensional, i.e. each tetrahedral sheet ordered independently of its neighbouring sheets. This therefore made it impossible on the time scale of our simulations for three-dimensional ordering across the whole sample to occur, on account of the large change required to shift the ordering patterns in adjacent layers with respect to one another. Indeed, the only way we were able to produce data pertaining to three-dimensional order was to start the simulation in an ordered arrangement and monitor the changes on heating. The only difference we recorded between the two-dimensional and three-dimensional cases was a different transition temperature, with the form of graphs of the order parameter, heat capacity and inverse susceptibility being similar for the two cases. It is therefore not especially instructive to include the interlayer interactions, and by analogy, in our study of phengite, we investigate only one T–O–T layer.

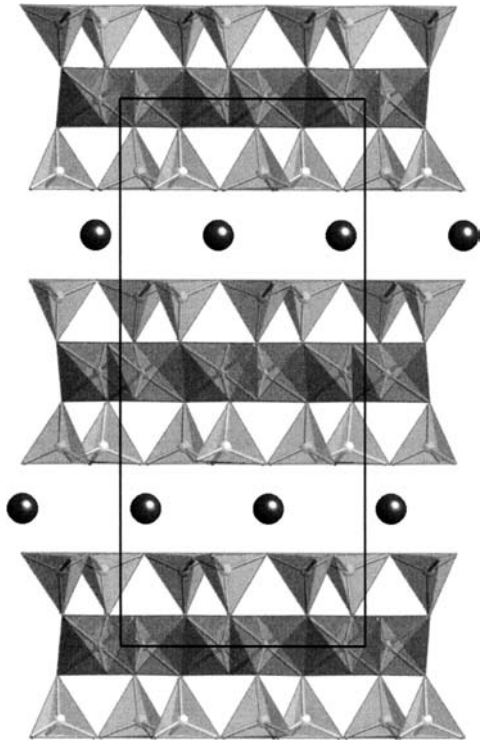

Fig. 1 Structure of phengite $2M_1$ viewed down the *a* axis. Two tetrahedral sheets and one octahedral sheet form a layer, and layers are separated by sheets of interlayer K^+ cations. The unit cell encompasses two layers (indicated by the *box*)

Methods

Basic strategy

Our method for simulating cation-ordering processes comprises two stages. Firstly, we determine values for ordering interactions by using empirical interatomic potentials and lattice energy relaxation methods. These values are then used to simulate ordering as a function of temperature using Monte Carlo simulations. Our approach uses a model Hamiltonian for the ordering interactions; we refer to this as the *J* formalism. We can write the energy of the system in terms of separate pair interactions for the three types of ordering cations present (Al, Mg and Si):

$$E = E_0 + \sum_n N^n_{\mathrm{Al-Al}}E^n_{\mathrm{Al-Al}} + N^n_{\mathrm{Si-Si}}E^n_{\mathrm{Si-Si}} + N^n_{\mathrm{Mg-Mg}}E^n_{\mathrm{Mg-Mg}} + N^n_{\mathrm{Si-Al}}E^n_{\mathrm{Si-Al}} + N^n_{\mathrm{Mg-Al}}E^n_{\mathrm{Mg-Al}} + N^n_{\mathrm{Mg-Si}}E^n_{\mathrm{Mg-Si}}\ , \quad (1)$$

where *n* indicates different types of neighbouring pairs of cations (for example, pairs with different separations), and the total energy is determined by summing over all types of interactions. E_0 is a constant term. It can be shown that this energy can also be expressed as

$$E = E'_0 + \sum_n N_{\mathrm{Al-Al}}(E^n_{\mathrm{Al-Al}} + E^n_{\mathrm{Mg-Si}} - E^n_{\mathrm{Al-Si}} - E^n_{\mathrm{Al-Mg}}) = E'_0 + \sum_n N^n_{\mathrm{Al-Al}}J_n\ , \quad (2)$$

where E_0' is a different constant term. The parameter J is called the exchange interaction parameter, and subsumes the separate energy terms for each pair of neighbours. The result we arrive at in Eq. (2) is identical to that derived for two types of ordering cations in our previous muscovite paper, except that the definition of J is different. This difference does not, however, affect our analysis.

Model interatomic potentials

As mentioned above, the first task in the investigation is to determine values for the J parameters, which we achieve by using empirical model interatomic potentials and relaxation of the lattice energy. Previous studies (e.g. Post and Burnham 1986; Patel et al. 1991; Winkler et al. 1991; Collins and Catlow 1992; Dove et al. 1993; Thayaparam et al. 1994) have shown that the modelling of crystal structures can be performed with fairly good accuracy using such potentials, with one study (Sainz-Díaz et al. 2001) showing this specifically for dioctahedral 2:1 phyllosilicates.

All ions in the model are modelled using formal charges, except the hydroxyl ions. The hydroxyl O and H ions have non-formal charge values which sum to the overall hydroxyl formal charge of $-1e$. We used four different types of interatomic potential in our model, for which the equations are given below. We use the general symbols E for energy, r for interatomic distance, and θ for an angle between two interatomic vectors, with a zero subscript indicating an equilibrium value.

Short-range interactions for Si–O, Al–O, K–O and O–O are modelled with Buckingham energy potentials:

$$E = A\exp(-r/\rho) - Cr^{-6} \quad , \tag{3}$$

with the parameter C having zero value in the case of Al–O and O–O. O–Si–O tetrahedral interactions and O–Al–O tetrahedral and octahedral interactions are modelled with three-body potentials:

$$E = \frac{1}{2}k(\theta - \theta_0)^2 \quad . \tag{4}$$

O–H interactions within the hydroxyl group are modelled using a Morse potential:

$$E = D\{(1 - \exp[-a(r - r_0)])^2 - 1\} \quad . \tag{5}$$

Finally, all non-hydroxyl O atoms are modelled by the shell model, where they are considered to consist of a core comprising the nucleus and tightly bound inner electrons, surrounded by a massless shell of the remaining outer electrons. The cores are allocated a charge of $+0.84819e$ and the shells a charge of $-2.84819e$, such that the formal charge for the ion is maintained. Core and shell are held together by a harmonic interaction of the form

$$E = \frac{1}{2}Kd^2 \quad , \tag{6}$$

where d is the core-shell separation.

The values of the parameters a, C, k etc. are taken from a variety of sources. The models have been tested for a wide range of layer silicates by Sainz-Díaz et al. (2001), and in our muscovite work (Palin et al. 2001). Details of the values used are given in Table 1.

Lattice energy calculations are performed with GULP (Gale 1997), where the electrostatic energy is summed by the Ewald method. The lattice energies are relaxed using the Newton–Raphson minimization method.

Model testing

The model we used was adapted from our muscovite model. We tested the model here by calculating the equilibrium structure assuming complete Al–Si disorder across the tetrahedral sites, and complete Al–Mg disorder across the octahedral sites. We compared the model to experimental data for the $2M_1$ polytype (Gueven 1971). In this structure, the formula unit is $K_2(Al_3Mg)(Si_7Al)O_{20}(OH)_4$, with lattice parameters $a = 5.2112$ Å, $b = 9.0383$ Å, $c = 19.9473$ Å, $\beta = 95.769°$. The hydrogen atoms were not located by Gueven, so they were added to the structure (before relaxation) at suitable positions to form hydroxyl groups. The relaxed structure had lattice parameters $a = 5.2479$ Å, $b = 9.1185$ Å, $c = 19.5295$ Å, $\beta = 96.880°$, respectively, which differ from the experimental values by 2.1% at most. The mean tetrahedral cation–O distance was 1.627 Å (experiment) and 1.637 Å (calculation), the

Table 1 Parameter values used in the interatomic potentials for phengite. The label O1 indicates the hydroxyl-forming oxygen atoms; O2 indicates all other oxygen atoms; O indicates both 01 and 02 atmos

Potential type	Atoms	Parameter values				
		A	ρ	C	r_{max}	
Buckingham	Si core–O1 core	999.9	0.3012	0	12	
Buckingham	Si core–O2 shell	1283.9077	0.3205	10.66	12	
Buckingham	Al core–O1 core	1460.3	0.29912	0	12	
Buckingham	Al core–O2 shell	1460.3	0.29912	0	12	
Buckingham	Mg core–O1 core	1428.5	0.2945	0	12	
Buckingham	Mg core–O2 shell	1428.5	0.2945	0	12	
Buckingham	K core–O shell	65269.7	0.213	0	12	
Buckingham	O shell–O shell	22764	0.149	27.88	12	
Buckingham	H core–O2 shell	325	0.25	0	12	
		D	a	r_0	r_{max}	
Morse	O1 core–H core	7.0525	2.1986	0.9485	1.4	
		K				
Spring (core–shell)	O core–O shell	74.92				
		k	θ_0	r_{max} (1–2)	r_{max} (2–3)	r_{max} (1–3)
Three-body	O shell–Si core–O shell	2.0972	109.47	1.8	1.8	3.2
Three-body	O shell–Al1 core–O shell	2.0972	109.47	1.95	1.95	3.4
Three-body	O shell–Al2 core–O shell	2.0972	90	2.2	2.2	3.2
Three-body	O shell–Mg core–O shell	2.0972	90	2.2	2.2	3.2

mean octahedral cation–O distance was 1.963 Å (experiment) and 1.910 Å (calculation), the mean octahedral cation–OH distance was 1.942 Å (experiment) and 2.073 Å (calculation) the mean K–O distance was 2.971 Å (experiment) and 2.963 Å (calculation) and the mean O–H distance was 0.976 Å (calculation, no experimental value given). There is good agreement for all distances, the worst being the octahedral cation–OH distances with a 7% discrepancy, but all other distances agree to within 2.5%.

Determination of the exchange interactions in phengite

Our model for phengite considers three different types of exchange interactions: tetrahedron–tetrahedron (T–T), octahedron–octahedron (O–O) and tetrahedron–octahedron (T–O). For the O–O interactions, we used values that had previously been used in smectites (sample 3 from Sainz-Díaz et al. 2003). For the T–T interactions we used values that we had previously used in muscovite, with the values having been slightly adjusted by setting $J_{3,T-T} = 0$. These values are given in Table 2.

For the T–O interactions, we examined the structure using MSI Cerius[2] and chose the four shortest different interatomic distances between atoms in the tetrahedral and octahedral sheets. We labelled these J_{a-d}. Figure 2 shows an octahedral sheet and one adjacent tetrahedral sheet, and the distances assigned. Additionally, Figures 3 and 4 show how the T–T and O–O interactions are assigned. The distances within the structure corresponding to the T–O interactions are given in Table 3.

The method we used for calculating the T–O interactions was as follows. We used a supercell with periodic boundary conditions, and calculated the energies of many different configurations with the ordering cations randomly located on different sites in each configuration. The supercell used was similar to the one used for muscovite – a $2 \times 2 \times 1$ supercell of the monoclinic *C*-centred cell, containing 64 tetrahedral sites and 32 octahedral sites.

We generated 100 configurations using a spreadsheet method (Bosenick et al. 2001), with 8 Al and 56 Si cations being placed on the tetrahedral sites, and 8 Mg and 24 Al being placed on the octahedral sites. We imposed the constraint that electrostatic charge balance should be preserved in each layer. Each of the 100 configurations was completely relaxed (atomic positions and lattice parameters) using GULP, the lattice energy minimization program. We used the lattice parameters obtained from the previous energy minimization run, in which the tetrahedral and octahedral sites were set up with partial occupancies of Al/Si and Al/Mg corresponding to complete disorder. The energy minimizations provided 100 different lattice energies, which form the E values in Eq. (2).

The spreadsheet method was used to generate the number of Al–Al interactions for each exchange pair for each configuration. Thus, we had 100 sets of values for N_{Al-Al}, and coupled with the E values, we could perform a linear regression fit to Eq. (2), to give values for J_n. In fact, for the regression procedure, we used only the energies and N_{Al-Al} values from the configurations which optimized successfully in GULP. We included the values of J_{1-4} (T–T) and J_{1-4} (O–O) in the regression, but allowed only the values of J_{a-d} to change during the fitting. The J values we obtained are given in Table 3. The agreement between values of the lattice energies of the different configurations and the corresponding values of the model Hamiltonian is shown in Fig. 5. The correlation coefficient R^2 was 0.67.

The values of the exchange constants J_{a-d} are typical of the range of values obtained for other aluminosilicates (e.g. Thayaparam et al. 1994, 1996; Dove et al. 2000), and following our earlier

Table 2 Values of atomic interaction parameters J for O–O and T–T interactions. T–T interactions adapted from Palin et al. (2001). O–O interactions-sample 3 from Sainz-Díaz et al. (2003)

Interaction type	Parameter	Value (eV)
T–T	J_1	1.01
T–T	J_2	0.2
T–T	J_3	0
T–T	J_4	0.14
O–O	J_1	0.6195
O–O	J_2	0.1510
O–O	J_3	0.0662
O–O	J_4	0.0297

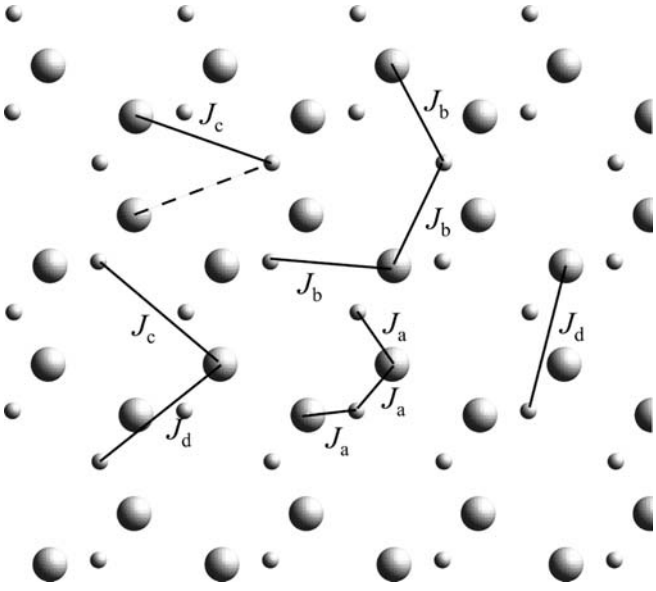

Fig. 2 Adjacent tetrahedral (large atoms) and octahedral (small atoms) sheets, showing the assigned J parameters for T–O interactions. The distances corresponding to the interactions are given in Table 3. The *dotted line* shows an interaction which appears from the Figure to be identical to J_c, but in fact its distance is larger than the cutoff we employed

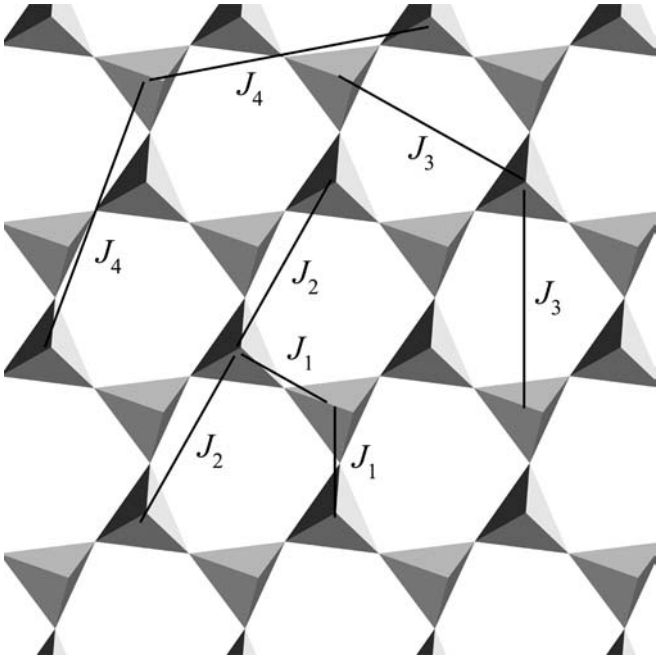

Fig. 3 Tetrahedral sheet showing assigned J parameters for T–T interactions

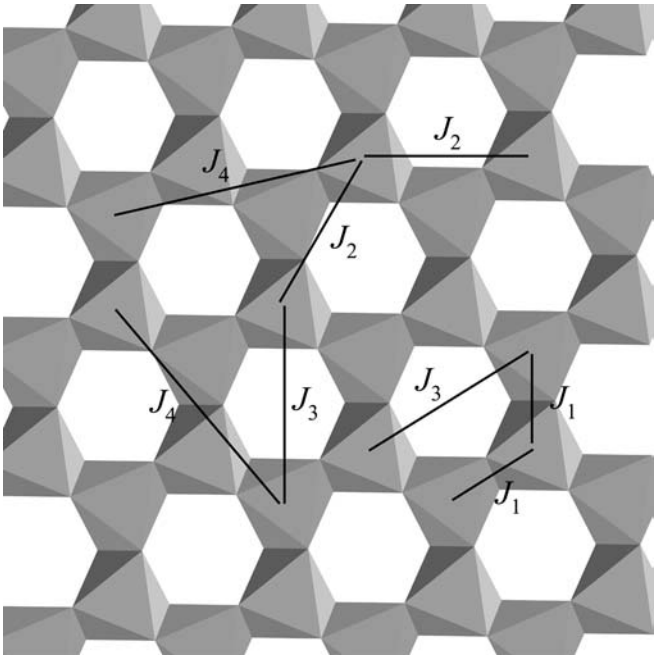

Fig. 4 Octahedral sheet showing assigned J parameters for O–O interactions

Table 3 Values of atomic interaction parameters for T–O interactions

Parameter	Distance (Å)	Value (eV)
J_a	3.10–3.23	0.75 (8)
J_b	4.37–4.60	0.06 (10)
J_c	5.27–5.42	0.02 (8)
J_d	5.13–5.24	0.24 (10)

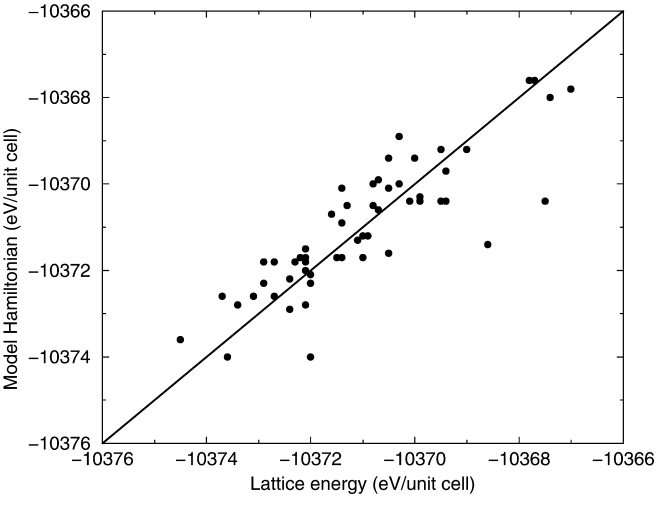

Fig. 5 Comparison of energies calculated from GULP and energies calculated from the model Hamiltonian using all Js illustrated in Figs. 2–4. The *straight line* indicates a perfect fit

work we obtain the result that the closest neighbour pair (Table 3) has the largest value of J. However, the fact that the value of J_a is positive is of interest. This means that Si_T–Al_O and Al_T–Mg_O pairs of atoms are preferred over Al_T–Al_O and Si_T–Mg_O pairs, where the subscripts T and O denote the sites on the tetrahedral and octahedral layers. If we were to consider only the effects of the electrostatic charges we might have presumed that the electrostatic interactions would prefer the latter set of pairings and hence give a negative value of J_a. Instead, we believe that the primary origin of the positive value of J_a arises from the effects of strain. It was shown by McConnell et al. (1997) that the primary component of the nearest-neighbour exchange interaction for Al/Si ordering in framework aluminosilicate structures is from strain, and a simple counting of charge distributions based on the use of formal changes suggests that the electrostatic interactions in this latter case are likely to be more significant than in the layer silicate being considered here. Usually, strain has the effect of preferring to have small cations interlaced with large cations in order to minimize the long-range strain. In the case of interactions between planes of atoms, it is more likely that the T–O pairs of atoms would be most easily accommodated if they are of the most similar size. This is because the strain effects on the two layers would be most closely matched, and the large–small interlace would be most useful operating only within the individual layers. If we had a small cation in one layer next to a large cation in the other layer, the small cation would pull its layer inwards and the large cation would push its layer outwards. There would then be a significant strain on the next neighbour pair which could not easily be accommodated by a different pair since the small Si and large Mg cations are confined to the tetrahedral and octahedral layers, respectively.

It should be noted that there is a difference between the results reported in this paper and the example calculations reported previously for phengite (Warren et al. 2001). In the latter study, the J values were calculated from a limited dataset, for the purpose of illustrating the method involved rather than arriving at exact results. The difference between the respective sets of J values generates a different ordered scheme, illustrating the sensitivity of such complex systems (see below).

Monte Carlo methods

In our previous study of muscovite we were able to inspect the J values and predict correctly the behaviour of the system from the fact that $J_3 \approx 0$ and $J_{1,2,4} > 0$. However, that study was of a single ordering scheme over one type of site, with the sites in a 2-D array. We do not expect, therefore, that it is as straightforward to predict the behaviour for phengite, where we are simulating simultaneously two ordering processes, over two different types of site, in a quasi-2-D array (quasi-2-D since we are modelling only one T–O–T layer). Instead, it may be broadly possible to suggest configurations which are unlikely (for example, the relatively large values of $J_{1,T-T}$, $J_{1,O-O}$ and $J_{a,T-O}$ may preclude the formation of Al–Al linkages over these distances where possible), but we are now modelling sufficiently complex systems for the Monte Carlo simulations to become our most useful predictive tool.

The Monte Carlo method can be applied to the study of cation ordering (Warren et al. 2001). We assign a variable S_j to each cation site, where $S_j = 1$ if the site is occupied by Al, and zero otherwise. Therefore, if we consider two sites, i and j, the product S_iS_j is 1 when the sites are both occupied by Al, and zero otherwise.

Thus, we can express the energy as the following Hamiltonian:

$$H = \sum_{\langle i,j \rangle} J_{ij} S_i S_j + \sum_i \mu_j S_j \ , \qquad (7)$$

where the first term is the energy associated with the bonds, and the second term is a chemical potential term. This term is necessary for modelling phengite, since we seek to prevent the presence of [6] Si and [4] Mg – there is no empirical evidence to show that any micas contain [6] Si, and although there exist some synthetic micas with [4] Mg, this has not yet been seen in phengites. We employ an artificial chemical potential in this work, such that placing Si on [6] or Mg on [4] causes a prohibitively large increase in the energy, but the method is equally valid for systems in which real chemical potentials have been evaluated.

We used our own MC program, Ossia. The program has been written for parallel computers and enables the simulation of a system at many different temperatures. More details can be found on the internet at http://www.esc.cam.ac.uk/ossia.

The output of the MC runs includes expectation values for the energy, $\langle E \rangle$ and $\langle E^2 \rangle$; and also for the order parameter, $\langle Q \rangle$ and $\langle Q^2 \rangle$. From these values it is possible to determine the heat capacity C and the susceptibility χ.

$$C = \frac{\langle E^2 \rangle - \langle E \rangle^2}{k_B T^2} \tag{8}$$

$$\chi = \frac{\langle Q^2 \rangle - \langle Q \rangle^2}{k_B T} \quad . \tag{9}$$

These quantities are useful in the study of phase transitions since they are indicators of the ordering temperature T_c. This temperature is defined as the point at which the order parameter falls to zero, but this can be difficult to measure accurately, since there are large fluctuations in Q close to T_c. At a second-order phase transition, the values of C and χ will diverge, which gives two further estimates of the value of T_c.

We define the order parameter in terms of the occupancies of both octahedral and tetrahedral sites, such that for complete disorder $Q = 0$, and for complete order $Q = 1$. The order parameter is set up as follows. If for a particular site j in the unit cell, the occupancy is s_j, with $s_{j,0}$ signifying the average occupancy at $T = 0$ in the ordered structure, and $s_{j,\infty}$ is the average occupancy as $T \to \infty$, the order parameter Q_j for this site is defined as:

$$Q_j = \frac{s_j - s_{j,\infty}}{s_{j,0} - s_{j,\infty}} \quad , \tag{10}$$

and then the overall order parameter over all sites in the unit cell is defined as:

$$Q = \frac{1}{n} \sum_j Q_j \quad , \tag{11}$$

where n is the total number of sites. It is important to note that the order parameter definition given here is for the non-symmetry-adapted order parameters that we obtain from Ossia, and not the transformed symmetry-adapted order parameters, which we discuss below.

Monte Carlo simulations of single tetrahedral sheet and single octahedral sheet in phengite

In our muscovite study we found that the ordered structure of a tetrahedral sheet with Al:Si = 1:3 was long-range-ordered with all Al–Al linkages as J_3. In this work, we have extended this by modelling the behaviour of a tetrahedral sheet with Al:Si = 1:7 as in phengite. Additionally, we performed simulations on an octahedral sheet with Al:Mg = 3:1 as in phengite.

The tetrahedral sheet simulation used only the T–T interactions, and the octahedral sheet simulation used only the O–O interactions. Each system consisted of 576 cation sites.

Examples of low-temperature output from these cooling runs are shown in Figs. 6 and 7.

The behaviour of the tetrahedral sheet is quite different from that in muscovite, in that it does not show any long-range order, although short-range order is present, with Al atoms being arranged over J_3 distances (Fig. 6). This is an example of Al/Si dilution (Dove et al. 1996; Myers et al. 1998). In a dilute system, it is easy for Al–Al linkages to be avoided, since the Al atoms can simply form a dispersed arrangement, meaning there is no requirement for long-range order.

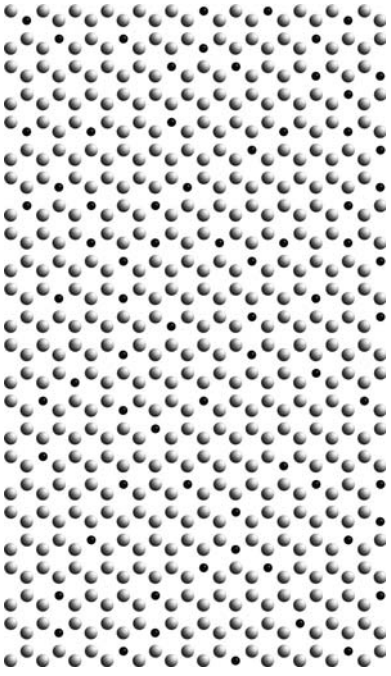

Fig. 6 Low-T configuration for simulation of one tetrahedral sheet. *Grey spheres* indicate Si atoms and *black spheres* Al atoms

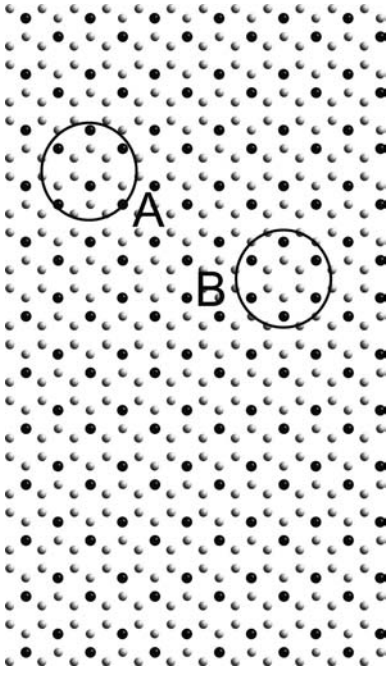

Fig. 7 Low-T configuration for simulation of one octahedral sheet. *Grey spheres* indicate Al and *black spheres* Mg. The pattern indicated at A is that formed due to long-range order, whilst that at B is the "superhexagon" structure, here formed due to the existence of a domain wall

The octahedral sheet (Fig. 7) has chains of Mg atoms in J_3 positions. This structure is related to the "superhexagon" structure seen in the tetrahedral sheet of muscovite (which had the same proportions of the ordering cations, albeit different species), except that the chains of J_3-linked Mg atoms are in phase rather than out of phase. There is evidence for both the in-phase and out-of-phase structures in Fig. 7, although the latter is only present along domain walls rather than being the dominant configuration. The presence of both structures is not surprising, since they are very similar in energy – a structure consisting completely of the in-phase chains has an energy of 0.8093 eV atom^{-1}, whilst that with out-of-phase chains has an energy of 0.8102 eV atom^{-1}.

Monte Carlo simulations of one T–O–T layer

Having modelled the tetrahedral and octahedral sheets independently, we next modelled a whole T–O–T layer. The model for this includes all of the T–T, O–O and T–O exchange interactions in Tables 2 and 3. We simulated one layer from a $12 \times 12 \times 1$ supercell of phengite (1152 T sites, 576 O sites).

From the output of the first run on phengite (Fig. 8) we made two observations. Firstly, Fig. 8 suggests that long-range order does not occur in a system with the phengite composition. Instead, Mg–Mg nearest-neighbour pairs form in the octahedral sheet, and the Al atoms in the tetrahedral sheet line up in J_a positions with respect to these pairs, forming a group of two Mg and two Al atoms. Figure 8 shows that the Mg atoms can line up in two ways – one such that an imaginary bond drawn between the two atoms in a pair would point vertically on the Figure, and the other such that it would point at an angle of approximately 120° to the vertical. These groups of Al and Mg line up with respect to one another, but it is not possible for them to occur across the whole unit cell for this composition.

Secondly, we observed from Fig. 8 that it is possible to define a new, smaller unit cell for the case of a perfectly ordered structure (i.e. one containing sufficient Mg and $^{[4]}$Al atoms to produce long-range order). Therefore, we redefined the unit cell in terms of this structure (see Fig. 9), thereby decreasing the number of T sites to 24 and the number of O sites to 12. The new supercell was then taken to be a $4 \times 8 \times 1$ multiple of this cell (768 T sites, 384 O sites).

These two observations led us to perform simulations on the system with a composition which should allow full order to occur, i.e. with 1/3 Mg and 2/3 Al on the O sites, and 1/6 Al and 5/6 Si on the T sites. This is not a mica end-member composition, but it can exist in a di-octahedral mica if the difference in total layer charge from phengite ($-2/3e$) is accommodated by substitution of M^{2+} for K^+ in the interlayer region.

Monte Carlo simulation of layer with long-range-ordered composition

A heating run was performed with the system being set up in the structure shown in Fig. 10. The resulting energy and heat capacity data are given in Fig. 11. Also shown are the data from a cooling run, which show the

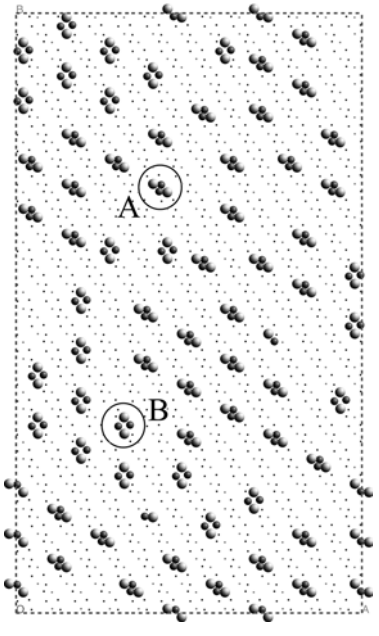

Fig. 8 Typical MC simulation output at low T for a whole phengite T–O–T layer cooling simulation, viewed down the c axis. Only the Al, Si and Mg atoms are shown, and of these, the $^{[4]}$Al and $^{[6]}$Mg are highlighted for contrast. *A* and *B* show the two ways of lining up the ordering units of 2 $^{[6]}$Mg atoms and 2 $^{[4]}$Al atoms

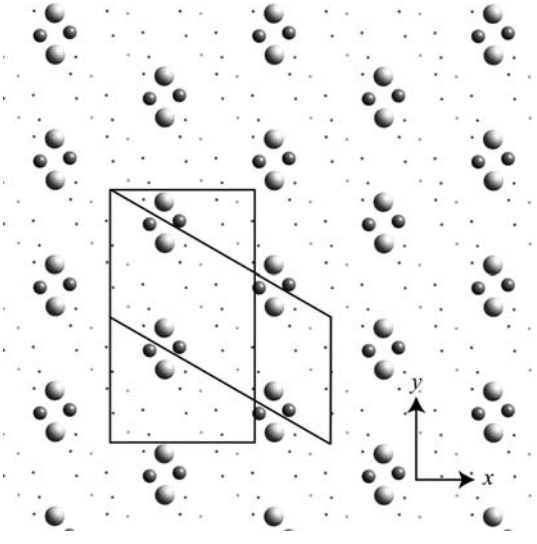

Fig. 9 Phengite T–O–T layer viewed down the c axis showing the relationship between old unit cell (*rectangle*) and new, smaller unit cell based on predicted ordering pattern (*parallelogram*). Only the Al, Si and Mg atoms are shown, and the highlighted atoms are $^{[6]}$Mg (*larger spheres*) and $^{[4]}$Al (*smaller spheres*)

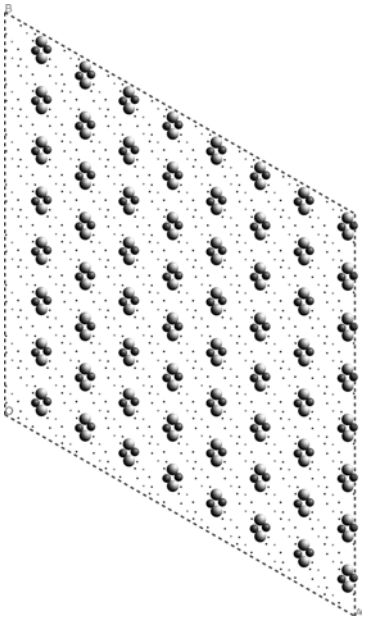

Fig. 10 Configuration of a long-range-ordered T–O–T layer viewed down the c axis. This layer has a necessarily different composition from that of phengite

same trend, apart from the problem of equilibration at lower temperature.

According to the two different orientations (A and B) of the Mg atoms in Fig. 8, we defined six order parameters $\{Q_i, i = 1, \ldots, 6\}$, corresponding to each of the six possible ordered states (there are six because for each orientation, there are three possible arrangements with respect to the unit cell).

The order parameters thus defined were linearly dependent, in that the six order parameters summed to zero, and hence only five of them need be declared, since the sixth can be inferred. These order parameters thus transform between each other forming a five-dimensional representation of the $3/m$ point group. However, the representation they form is not irreducible in the group-theoretical sense and thus they are not order parameters in the Landau sense (they are not symmetry-adapted). Therefore we decomposed the Q_i into order parameters $\{\eta_i, i = 1, \ldots, 3\}$, corresponding to the irreducible representations A′, E′ and E″ of the $3/m$ symmetry group. The first representation is one-dimensional, the latter two are two-dimensional, with real and imaginary components labelled (1) and (2). The transformation from one set of order parameters to the other is given by

$$\begin{bmatrix} \eta_1 \\ \eta_2^{(1)} \\ \eta_2^{(2)} \\ \eta_3^{(1)} \\ \eta_3^{(2)} \end{bmatrix} = \begin{bmatrix} 1 & 1 & 1 & 0 & 0 \\ 0 & \frac{3}{2} & 0 & 0 & \frac{3}{2} \\ \sqrt{3} & \frac{\sqrt{3}}{2} & 0 & \sqrt{3} & \frac{\sqrt{3}}{2} \\ -1 & \frac{1}{2} & -1 & 0 & -\frac{3}{2} \\ 0 & -\frac{\sqrt{3}}{2} & -\frac{\sqrt{3}}{2} & -\sqrt{3} & -\frac{\sqrt{3}}{2} \end{bmatrix} \begin{bmatrix} Q_1 \\ Q_2 \\ Q_3 \\ Q_4 \\ Q_5 \end{bmatrix} . \tag{12}$$

The same transformation law may also be used on the susceptibilities.

The order parameter data were transformed in the manner described above, along with data for the susceptibility. The results for the order parameters and the inverse susceptibility are given in Fig. 12 and, from these, we can observe that the order–disorder phase transition occurs at approximately 1900 K. Order parameter and inverse susceptibility data are not shown for the cooling run, but long-range order is achieved on cooling (with the same problem of equilibration at low T). The form of the order parameter as a function of temperature is fairly similar to that obtained for muscovite, to which a 2-D Ising model was found to apply (with a critical exponent β of 1/8). We did not perform a detailed analysis of critical exponents, but a brief analysis of the data suggested a value for β of between 0.16 and 0.28, which is nearer the 2-D Ising model value than the second-order Landau model value of $\beta = 1/2$.

We investigated the presence of coupling between order parameters by plotting the squared η values against each other (we used the squared values because

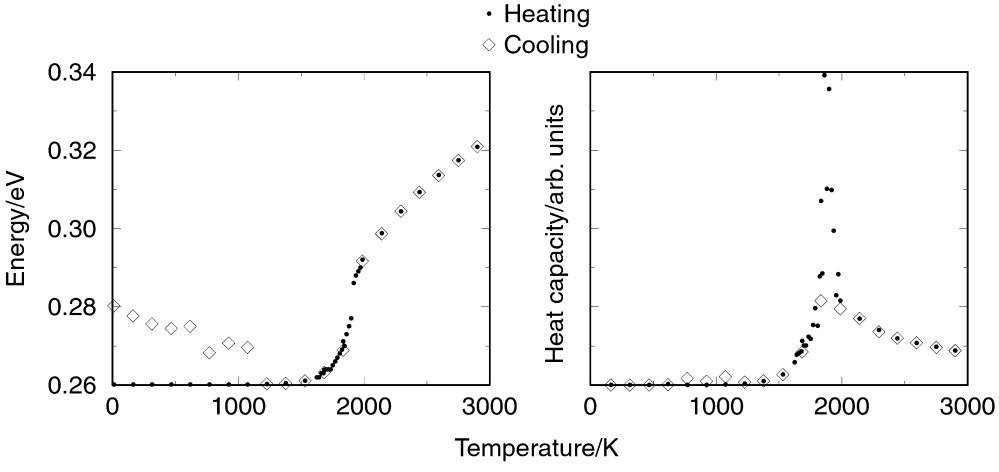

Fig. 11 Energy and heat capacity data for simulations (heating and cooling) using the new unit cell with the long-range-ordering composition. The problem of equilibration at low T is illustrated in the energy data by the different behaviour of the heating and cooling simulations

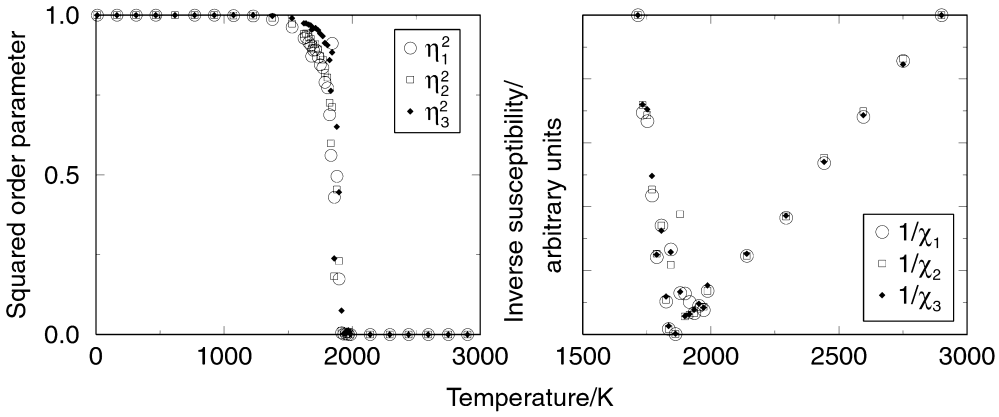

Fig. 12 Order parameter data and inverse susceptibility data (*scaled on either side of the phase transition*) for the long-range-ordering composition

of the complex character of η_2 and η_3). This is illustrated in Fig. 13, which shows that η_1 and η_2 are linearly coupled, whilst η_3 is the fundamental order parameter, since it is quadratically coupled with the other two order parameters. Hence, free energy expression for the system would have the following form (neglecting constants):

$$F = \eta_1^2 + \eta_2^2 + \eta_3^2 + \eta_1\eta_3^2 + \eta_2\eta_3^2 + \eta_1\eta_2 \ ,$$

whence it is clear that if η_3 changes, the fourth and fifth terms also change value.

Although long-range order occurs in the system with this composition, it is instructive to quantify the degree of short-range order, as this provides a framework within which to compare this composition with the phengite composition. The short-range order may be quantified by counting the number of various types of atomic interactions, as a function of temperature. Important interactions in the system are $J_{1,O-O}^{Mg-Mg}$ and $J_{a,T-O}^{Al-Mg}$, since these determine the configurations of the groups of two Al and two Mg atoms which are characteristic of the ordering scheme. Figure 14 shows these data, normalized such that perfect short-range (and therefore long-range) order corresponds to a value of unity, and complete disorder corresponds to a value of zero, although it is possible that there will be values outside this range. From Fig. 14 it can be seen that the short-range order in the system begins to decrease just below T_c.

Monte Carlo simulation of layer with phengite composition

Having determined the existence of long-range order in the T–O–T system described above, we returned to the whole-layer simulation of the phengite composition. We expected the ordering to be related to that in the long-range-ordered system and thus we converted the system to a smaller unit cell in a similar fashion. We were also able, therefore, to use the same order parameters, and the same transformations of the order parameters and susceptibilities.

It was not possible to perform heating and cooling runs in the usual manner on the phengite composition, since the long-range-ordered structure (on which the order parameters are based) has a different composition from phengite. Instead, we used an additional adaptation of the Ossia code, which enables the simulation of partial order, by starting the system in the perfectly ordered structure and randomly changing atoms of one species to those of another, until the desired overall composition (phengite) is achieved. Because of this, we do not expect the order parameters to approach unity at low temperature.

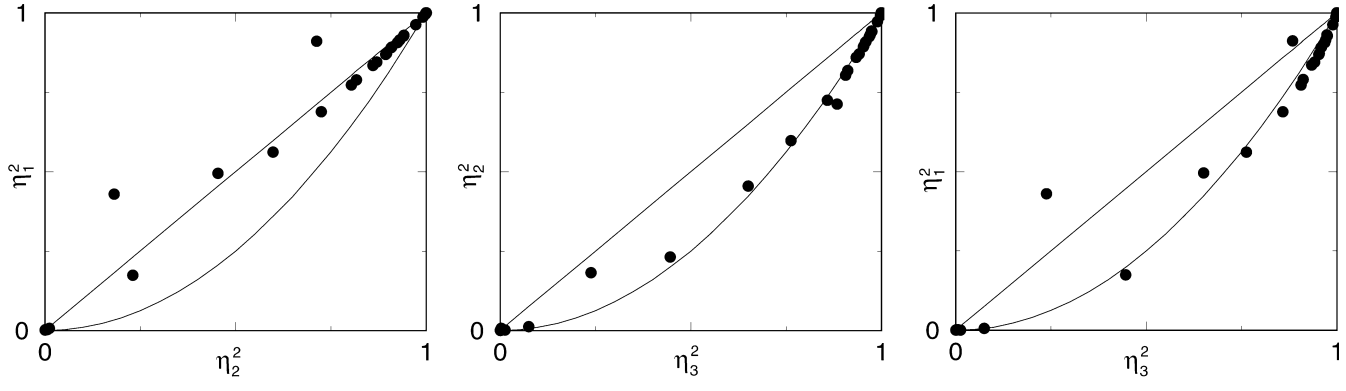

Fig. 13 Plots illustrating coupling between order parameters. Ideal linear and quadratic coupling relationships are shown on each graph

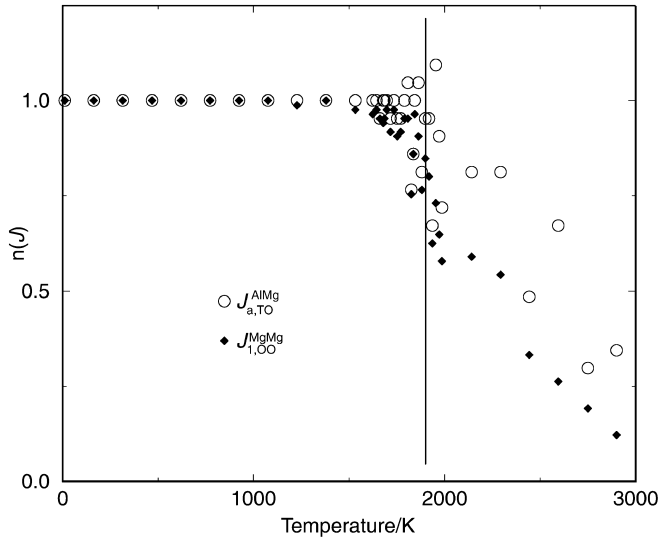

Fig. 14 Plot of $J_{1,O-O}^{Mg-Mg}$ and $J_{a,T-O}^{Al-Mg}$, indicating short-range order, for the long-range-ordering composition. The approximate value of T_c is marked by a *vertical line*

A typical output from a cooling simulation on the new unit cell is shown in Fig. 15. As expected, it shows the same features as Fig. 8.

We plot the energy and heat capacity of the system in Fig. 16. The form of the curves is different from that in Fig. 11 – there is no sharp feature in the heat-capacity profile, due to the lack of long-range order. Figure 17 shows the order parameter and susceptibility data. These data show that the phase transition in phengite occurs at approximately 1400 K. Again, this is a dilution effect; phengite has a more dilute Al:Si ratio than the long-range-ordered composition, and hence T_c is lower.

As expected, the order parameter does not approach unity in the system because of the lack of long-range order – the system attempts to create the long-range-ordered structure, but is only able to form short-range-ordered domains, often in more than one of the six possible configurations in Fig. 18. There are regions which are free from $^{[4]}$Al and $^{[6]}$Mg as a result.

A plot similar to that in Fig. 14 for phengite is shown in Fig. 19. As in Fig. 14, the short-range order begins to decrease just below T_c.

Concluding remarks

It is not straightforward to compare our results with X-ray and neutron diffraction experiments, since the majority of our findings indicate short-range order, whilst these techniques are chiefly probes of long-range order. In contrast, ^{29}Si MAS–NMR experiments are a good method of probing short-range order in the tetrahedral sheets, and have been performed on a variety of natural and synthetic 2:1 phyllosilicates (Lipsicas et al. 1984; Herrero et al. 1985, 1987; Sanz 1988; Circone et al. 1991). In one synthetic sample with $x_{Al} = 0.12$ (i.e.

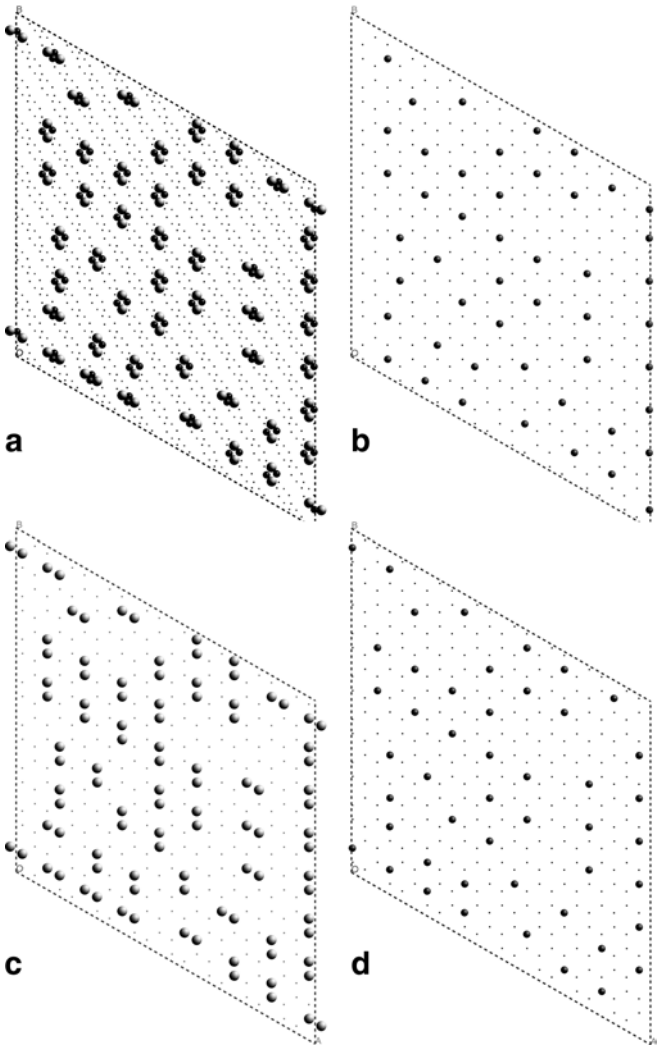

Fig. 15a Typical MC simulation output at low T for simulation of phengite, using the new unit cell. $^{[6]}$Mg (*larger spheres*) and $^{[4]}$Al (*smaller spheres*) highlighted. **b–d** show the T, O, T sheets in **a** separately, for clarity

roughly that of phengite), the spectra indicated 39% Si–2Si1Al, 61% Si–3Si in the tetrahedral sheet. In a tetrahedral configuration such as that shown in Fig. 6, the proportions are approximately 42% Si–2Si1Al, 58% Si–3Si, which is in reasonable agreement with the experimental data. However, if one considers the rather different tetrahedral configuration in Fig. 15b and d, almost the same proportions are obtained. This suggests, therefore, that ^{29}Si MAS–NMR analysis to investigate tetrahedral order in phengite would not be conclusive.

There is some weak evidence for low degrees of octahedral cation ordering in phengite $3T$ and $2M_1$ polytypes (Pavese et al. 1997, 2000, 2001). However, in their latest paper these authors themselves present their results rather cautiously, pointing out that they might also be a consequence of structural defects such as stacking faults. Nonetheless, our computational results indicate moderate sized (~25–50 Å) domains of cation order within the octahedral sheets, and the neutron diffraction

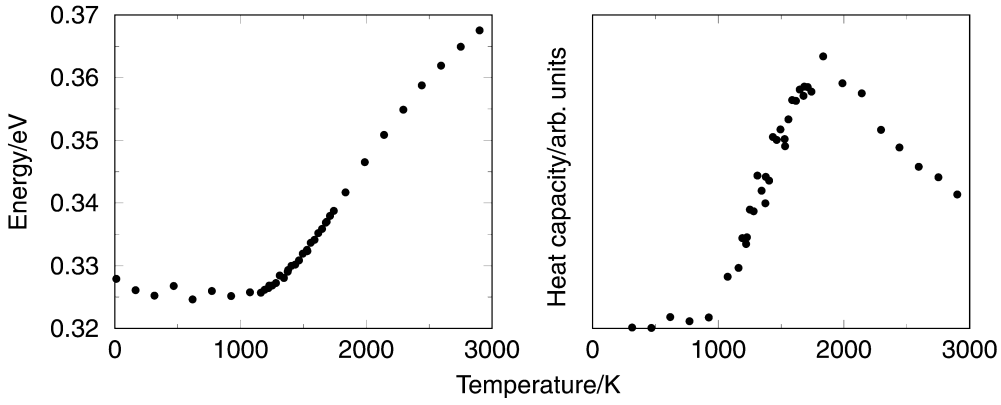

Fig. 16 Energy and heat capacity data for a simulation of phengite, using the new unit cell

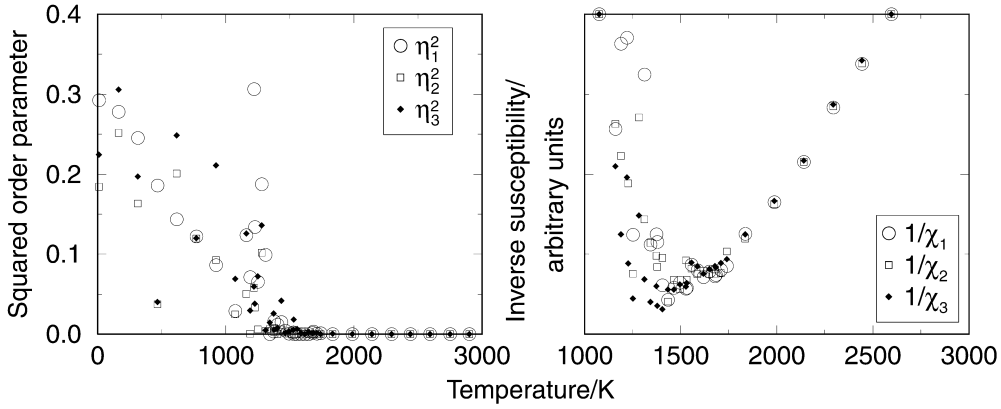

Fig. 17 Order parameter data and inverse susceptibility data (*scaled on either side of the phase transition*) for phengite

results of Pavese and coworkers may be a reflection of such medium-range order. One might anticipate that any kinetic hindrance to the development of long-range order in natural samples would modify the actual measured values of LRO in diffraction experiments.

In any case, our simulations have provided an insight into what is clearly a complicated mineral system. We have used the T–O interactions computed in this work in conjunction with the T–T and O–O interactions determined for similar minerals, to suggest the presence of short-range order in phengite. The system attempts to avoid as many Al–Al interactions as possible being formed over nearest-neighbour T–T distances, by creating a dispersed arrangement of Al atoms, which is easily

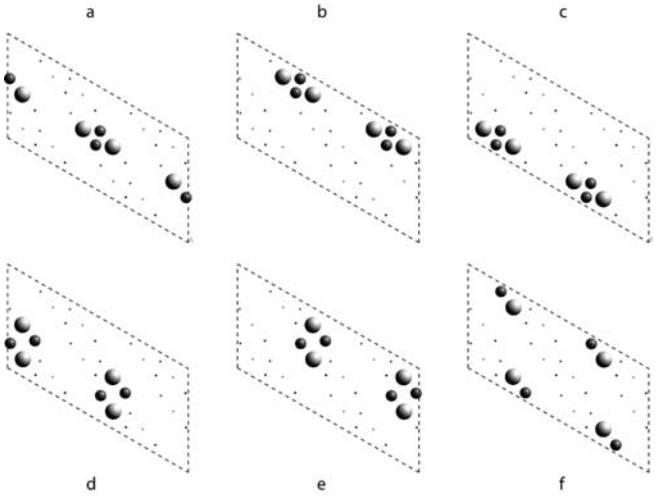

Fig. 18 The six possible ordered configurations in the new unit cell. **a**–**c** are equivalent, and **d**–**f** are equivalent, the difference between equivalent configurations being simply the choice of unit-cell origin

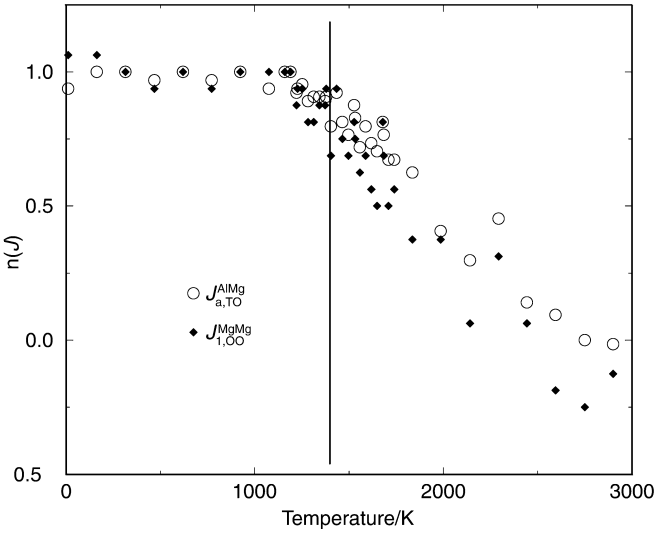

Fig. 19 Plot of $J_{1,O-O}^{Mg-Mg}$ and $J_{a,T-O}^{Al-Mg}$, indicating short–range order, for phengite. The approximate value of T_c is marked by a *vertical line*

achieved due to the low Al:Si ratio. Nearest-neighbour T–O Al–Al linkages are avoided by creating Al–Mg linkages between the tetrahedral and octahedral sheets. It is interesting to note, however, that in the octahedral sheets, the system could decrease the number of Al–Al nearest-neighbour linkages by distributing the Mg atoms over non-nearest-neighbour distances, but this does not happen. From this information, then, it appears that the dominant interactions controlling ordering in phengite are the nearest-neighbour T–T and nearest-neighbour T–O interactions. We have shown that modelling the system with the T–O interactions gives different results from modelling the T and O systems independently.

Finally, we have shown analogous results for a mica composition which orders perfectly, although this is not an end-member composition, in order to illustrate the different thermodynamic behaviour between systems with short- and long-range order.

Acknowledgements The authors are grateful to EPSRC (EJP) and the Royal Society (CIS) for financial support. Monte Carlo simulations were performed on the Mineral Physics Group's Beowulf cluster and the University of Cambridge's High Performance Computing Facility.

References

Bosenick A, Dove MT, Myers ER, Palin EJ, Sainz-Díaz CI, Guiton B, Warren MC, Craig MS, Redfern SAT (2001) Computational methods for the study of energies of cation distributions: applications to cation-ordering phase transitions and solid solutions. Mineral Mag 65: 193–219

Circone S, Navrotsky A, Kirkpatrick RJ, Graham C (1991) Substitution of $^{[6,4]}$Al in phlogopite: mica characterization, unit-cell variation, ^{27}Al and ^{29}Si MAS-NMR spectroscopy, and Al–Si distribution in the tetrahedral sheet. Am Mineral 76: 1485–1501

Collins DR, Catlow CRA (1992) Computer simulation study of structures and cohesive properties of micas. Am Mineral 77: 1172–1181

Dove MT, Cool T, Palmer DC, Putnis A, Salje EKH, Winkler B (1993) On the role of Al–Si ordering in the cubic-tetragonal phase transition of leucite. Am Mineral 78: 486–492

Dove MT, Thayaparam S, Heine V, Hammonds K (1996) The phenomenon of low Al/Si ordering temperatures in aluminosilicate framework structures. Am Mineral 81: 349–362

Dove MT, Bosenick A, Myers ER, Warren MC, Redfern SAT (2000) Modelling in relation to cation ordering. Phase Transitions 71: 205–226

Gale JD (1997) GULP: a computer program for the symmetry-adapted simulation of solids. J Chem Soc Faraday Trans 93: 629–637

Gueven N (1971) The crystal structures of $2M_1$ phengite and $2M_1$ muscovite. Z Kristallogr 134: 196–212

Herrero CP, Sanz J, Serratosa JM (1985) Tetrahedral cation ordering in layer silicates by ^{29}Si NMR spectroscopy. Solid State Commun 53: 151–154

Herrero CP, Gregorkiewitz M, Sanz J, Serratosa JM (1987) ^{29}Si MAS–NMR spectroscopy of mica-type silicates: observed and predicted distribution of tetrahedral Al–Si. Phys Chem Miner 15: 84–90

Ivaldi G, Ferraris G, Curetti N, Compagnoni R (2001) Coexisting $3T$ and $2M_1$ polytypes of phengite from Cima Pal (Val Savenca, western Alps): chemical and polytypic zoning and structural characterisation. Eur J Mineral 13: 1025–1034

Lipsicas M, Raythatha RH, Pinnavaia TJ, Johnson ID, Geise RF Jr, Costanzo PM, Robert J-L (1984) Silicon and aluminium site distributions in 2:1 layered clays. Nature 309: 604–607

McConnell JDC, DeVita A, Kenny SD, Heine V (1997) Determination of the origin and magnitude of Al/Si ordering enthalpy in framework aluminosilicates from ab initio calculations. Phys Chem Miner 25: 15–23

Mookherjee M, Redfern SAT, Zhang M (2001) Thermal response of structure and hydroxylation of phengite $2M_1$: an in situ neutron diffraction and FTIR study. Eur J Mineral 13: 545–555

Myers ER, Heine V, Dove MT (1998) Thermodynamics of Al/Al avoidance in the ordering of Al/Si tetrahedral framework structures. Phys Chem Miner 25: 457–464

Palin EJ, Dove MT, Redfern SAT, Bosenick A, Sainz-Díaz CI, Warren MC (2001) Computational study of tetrahedral Al–Si ordering in muscovite. Phys Chem Miner 28: 534–544

Patel A, Price GD, Mendelssohn MJ (1991) A computer-simulation approach to modelling the structure, thermodynamics and oxygen isotope equilibria of silicates. Phys Chem Miner 17: 690–699

Pavese A, Ferraris G, Prencipe M, Ibberson R (1997): Cation site ordering in phengite 3T from the Dora Maira Massif (Western Alps) – a variable temperature neutron powder diffraction study. Eur J Mineral 9: 1183–1190

Pavese A, Ferraris G, Pischedda V, Ibberson R (1999): Tetrahedral order in phengite $2M_1$ upon heating, from powder neutron diffraction, and thermodynamic consequences. Eur J Mineral 11: 309–320

Pavese A, Ferraris G, Pischedda V, Radaelli P (2000): Further study of the cation ordering in phengite 3T by neutron powder diffraction. Mineral Mag 64: 11–18

Pavese A, Ferraris G, Pischedda V, Fauth F (2001): M1-site occupancy in 3T and $2M_1$ phengites by low temperature neutron powder diffraction: reality or artefact? Eur J Mineral 13: 1071–1078

Post JE, Burnham CW (1986) Ionic modelling of mineral structures and energies in the electron gas approximation: TiO_2 polymorphs, quartz, forsterite, diopside. Am Mineral 71: 142–150

Sainz-Díaz CI, Hernández-Laguna A, Dove MT (2001) Modelling of dioctahedral 2:1 phyllosilicates by means of transferable empirical potentials. Phys Chem Miner 28: 130–141

Sainz-Díaz CI, Palin EJ, Dove MT, Hernández-Laguna A (2003) Ordering of Al, Fe and Mg cations in the octahedral sheet of smectites and illites by means of Monte Carlo simulations. Am Mineral (in press)

Sanz J (1988) Distribution of ions in phyllosilicates by NMR spectroscopy. In: Mottana A, Burragato F, (eds) Absorption spectroscopy in mineralogy. Elsevier, Amsterdam, pp 103–144

Sassi PF, Guidotti C, Rieder M, De Pieri R (1994): On the occurrence of metamorphic $2M_1$ phengites: some thoughts on polytypism and crystallization conditions of 3T phengites. Eur J Mineral 6: 151–160

Thayaparam S, Dove MT, Heine V (1994) A computer simulation study of Al/Si ordering in gehlenite and the paradox of the low transition temperature. Phys Chem Miner 21: 110–116

Thayaparam S, Heine V, Dove MT, Hammonds KD (1996) A computational study of Al/Si ordering in cordierite. Phys Chem Miner 23: 127–139

Warren MC, Dove MT, Myers ER, Bosenick A, Palin EJ, Sainz-Díaz CI, Guiton B, Redfern SAT (2001) Monte Carlo methods for the study of cation ordering in minerals. Mineral Mag 65: 221–248

Winkler B, Dove MT, Leslie M (1991) Static lattice energy minimization and lattice dynamics calculations on aluminosilicate minerals. Am Mineral 76: 313–331